

# On the Implementation Security of Twin-Field Quantum Key Distribution using Optical Injection Locking

Sergio Juárez,<sup>1, 2, \*</sup> Alessandro Marcomini,<sup>3, 2, 4, \*</sup> Mikhail Petrov,<sup>3, 2, 4</sup> Robert I. Woodward,<sup>1</sup> Toby J. Dowling,<sup>1</sup> R. Mark Stevenson,<sup>1</sup> Marcos Curty,<sup>3, 2, 4</sup> and Davide Rusca<sup>3, 2, 4</sup>

<sup>1</sup>*Toshiba Europe Limited, 208 Cambridge Science Park, Cambridge CB4 0GZ, UK*

<sup>2</sup>*Escuela de Ingeniería de Telecomunicación, Department of Signal*

*Theory and Communications, University of Vigo, Vigo E-36310, Spain*

<sup>3</sup>*Vigo Quantum Communication Center, University of Vigo, Vigo E-36310, Spain*

<sup>4</sup>*AtlanTTic Research Center, University of Vigo, E-36310, Spain*

Twin-Field Quantum Key Distribution (TF-QKD) has emerged as a leading quantum communication protocol, enabling secure key distribution over unprecedented distances by utilising coherent interference of quantum states. Optical Injection Locking (OIL) architectures have been used to simplify the precise phase and frequency stabilisation required by TF-QKD. In this work, we systematically analyse potential side-channels in OIL-based TF-QKD that can be introduced through the various optical degrees of freedom of the externally injected reference laser. We experimentally demonstrate two realistic attack scenarios: rapid intensity modulation of the reference laser and Trojan-horse signals exploiting wavelengths undetectable by conventional monitoring techniques. To counter these vulnerabilities, we propose straightforward and highly effective countermeasures including high-speed photodiodes for real-time power monitoring and targeted spectral filtering to detect and suppress out-of-band signals. Our experimental results confirm that these practical solutions substantially reinforce the security of TF-QKD systems without significant additional complexity or performance degradation. More broadly, our analysis highlights the critical importance of comprehensive optical monitoring to ensure the robust practical deployment of TF-QKD in real-world quantum communication networks.

## INTRODUCTION

Quantum key distribution (QKD) enables two legitimate parties, Alice and Bob, to share a symmetric encryption key that can be used to achieve information-theoretically secure communications. In particular, it exploits the laws of quantum mechanics to ensure that any eavesdropping attempt by a malicious external party (Eve) cannot go undetected [1–4].

To date, QKD has matured into a well-established technology whose application has been demonstrated on the level of inter-city networks. Next-generation protocols such as twin field QKD (TF-QKD), which utilise single-photon interference, offer significantly improved resilience against channel losses [5–8], effectively doubling the achievable communication distances [9, 10], reaching up to 1000 km point-to-point [11–15]. These properties make TF-QKD particularly attractive for the realisation of nationwide quantum networks [16–20].

Nevertheless, the broader adoption of QKD still faces some challenges, particularly the need to guarantee the security of practical implementations, since real devices inevitably deviate from the idealised assumptions. These deviations must be accounted for, either through improved security proofs or through enhancements in physical hardware, a domain collectively known as implementation security [21, 22]. Unaddressed device imperfections can lead to unintended side channels, resulting in

undetected information leakage which may compromise the overall system security [23–25].

In this regard, TF-QKD possesses a crucial advantage, as it belongs to the measurement-device-independent (MDI) class of protocols. MDI protocols remove all security assumptions from the receiver, ensuring security even if Eve completely controls the measurement apparatus [26]. Consequently, implementation security efforts can be entirely focused on the transmitter side.

Practical implementations of TF-QKD require a shared phase and frequency reference between Alice's and Bob's encoders. Typically, this reference is provided by the untrusted central measurement node (Charlie), which distributes a classical reference beam through a dedicated service channel. The received beam stabilises the laser sources via optical phase-locked loops (OPLLs) or, more commonly, optical injection locking (OIL) [27–29]. OIL is particularly favoured due to its inherent stability, practicality, and lack of necessity for active feedback control [16, 30]. However, permitting an external beam, potentially altered by Eve en route, to directly enter the encoders raises critical concerns regarding implementation security [24, 31, 32].

In this work, we provide the first thorough analysis of implementation security specifically tailored to the OIL architecture used in TF-QKD. We investigate potential attack scenarios enabled by manipulation of the reference laser, examining multiple optical degrees of freedom and revealing two new potential side channels. Additionally, we also provide practical countermeasures for them.

The first side channel exploits rapid intensity modulation of the reference laser, performed faster or on the

\* These two authors contributed equally

same timescale as pulse encoding, temporarily increasing the emitted photon number without detection by conventional monitoring. The second side channel exploits back-reflections from the laser diode (LD) and the limited spectral response of monitoring devices. This allows Eve to embed a Trojan wavelength within the reference beam, possibly leaking the complete information about the intensity and phase encoding settings.

Our analysis underscores the necessity for careful spectral filtering of the injected reference beam and highlights the importance of employing monitoring systems (“watchdogs”) that track the timing and integrity of the incoming signals with high temporal resolution. Implementing these countermeasures effectively closes these side channels, significantly strengthening the security of OIL TF-QKD implementations.

The remainder of this paper is structured as follows: first, we provide a detailed examination of potential attack vectors originating from Eve’s manipulation of Charlie’s reference signal, identifying rapid intensity modulation and out-of-band Trojan signals as realistic threats. Next, we experimentally demonstrate the feasibility of these attacks and evaluate suitable countermeasures. Finally, we present our conclusions and broader implications of our findings for the practical security of TF-QKD.

## I. POTENTIAL SIDE CHANNELS IN OIL TF-QKD

In Fig. 1(a), we present a simplified schematic of a typical TF-QKD system consisting of Alice, Bob, and Charlie. The central node (Charlie) provides a coherent optical reference to the transmitters (Alice and Bob) through the service channel. Alice and Bob individually prepare quantum states, which are subsequently sent back to Charlie via the quantum channel for single-photon interference and measurement. Both channels can potentially be manipulated by Eve, and, in the worst case, Charlie himself could be entirely under Eve’s control. Fig. 1(b) details the most important components of an encoder and receiver within an OIL-based TF-QKD architecture. The optical reference received from Charlie first passes through a polarisation controller (PC) and a polarising beam splitter (PBS), ensuring single-polarisation injection to optimise the injection-locking efficiency. The optical reference goes then through a circulator and is injected into the encoder’s laser, locking its emission with that of Charlie’s laser. This results in a shared optical frequency and a fixed phase offset, which enables coherent operation across all sources. Subsequently, the locked signal passes through the encoder, which uses intensity and phase modulators to craft the train of pulses through pulse carving and manual (active) phase randomisation. Finally, the pulses get attenuated to the single-photon level using a variable optical attenuator (VOA) and are transmitted back to Charlie after passing through an iso-

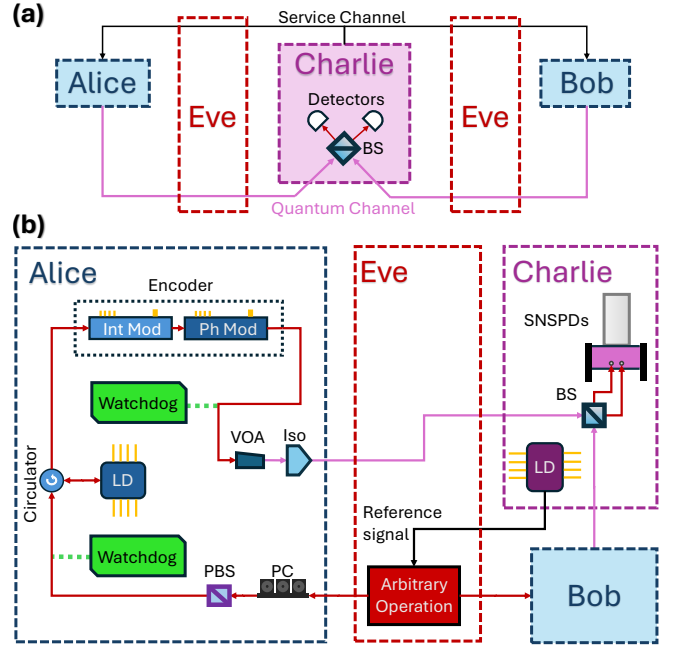


FIG. 1. Schematics of a basic TF-QKD system and encoder architecture based on OIL. (a) Overview of a typical TF-QKD setup where Charlie distributes a coherent reference via the service channel. Alice and Bob encode quantum signals and send them back through the quantum channel for interference at Charlie’s BS and measurement. Eve can manipulate both channels and, in the most extreme case, take full control of Charlie. (b) Key components of an OIL-based encoder. The reference passes through a PC and PBS for single-polarisation injection, then locks the local LD via a circulator. The output is encoded using an intensity modulator (Int Mod) and phase modulator (Ph Mod), attenuated to the single-photon level with a VOA, and sent to Charlie through an isolator (Iso). Interference and detection are performed at Charlie using a BS and single-photon detectors such as SNSPDs. The watchdogs guarantee the integrity of these signals. Bob’s setup is identical to Alice’s.

lator that prevents attacks from the quantum channel against the transmitter.

This architecture simplifies frequency and phase stabilisation, ensuring coherent interference at Charlie’s measurement node. However, adversaries might attempt to exploit any of the various degrees of freedom of the injected reference signal, such as polarisation, phase, intensity, or wavelength (frequency), to gain information through side-channel attacks.

Polarisation-based attacks are mitigated by the PBS at the input of the security perimeter, which transmits a single polarisation component while suppressing the orthogonal one with a typical extinction ratio of 30 dB. As a result, polarisation attacks relying on rapid fluctuations of the polarisation of the reference beam lose one projection, while the remaining accepted component only fluctuates in intensity. Consequently, polarisation attacks become equivalent to intensity attacks. Phase

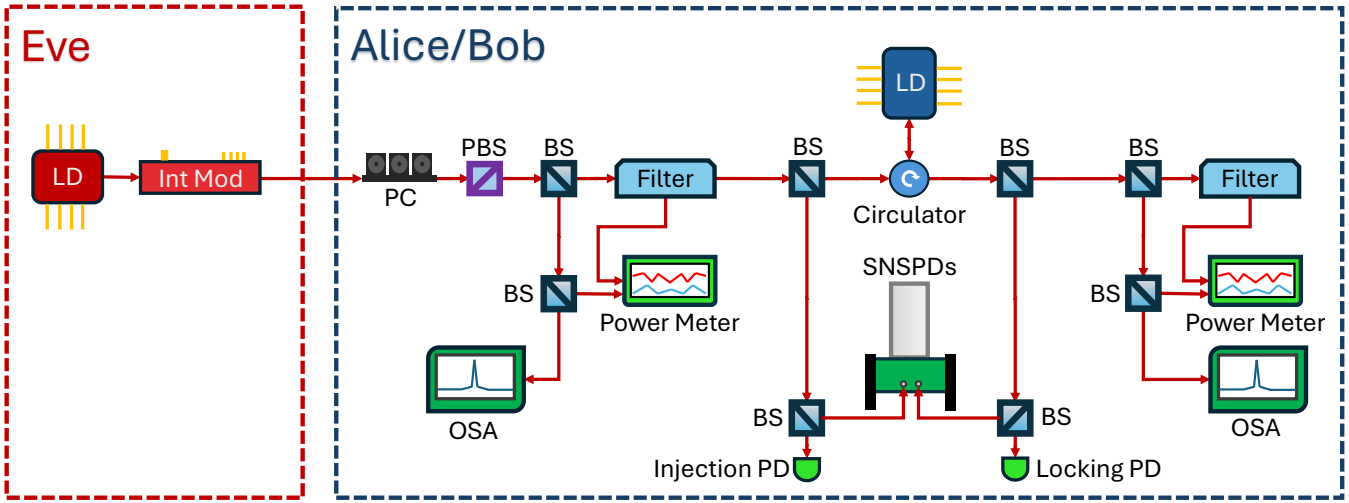


FIG. 2. **Experimental setup for studying the intensity modulation attack.** Here, Eve is assumed to fully control the intensity of the reference laser, implemented using an intensity modulator (Int Mod). The modulated reference signal enters Alice (or Bob), passing through a PC and a PBS, then undergoes spectral filtering to isolate the agreed reference from extrinsic wavelengths before injection-locking the LD. The behaviour of the injected and locked signals is characterised by SNSPDs and an OSA. The signals are also monitored by two PDs with GHz detection bandwidths, one to observe the signal injected into the encoder's laser (Injection PD) and another to monitor the laser's output after locking (Locking PD), and a power meter that checks filtered and unfiltered signals before and after the locking. After the second filter, the signal would normally pass through the encoder, be attenuated, and then sent to Charlie, as in in Fig. 1(b).

manipulation attacks are ineffective due to the active phase randomisation in Alice's and Bob's encoders after the OIL stage, and any excessive phase fluctuations are detectable as they will increase the quantum bit error rate (QBER), resulting at most in a denial-of-service scenario.

Intensity-based attacks present a threat to the single-photon level encoding of QKD. A rapid intensity modulation of the reference laser could potentially empower Eve to induce transient increases in the output power of Alice's and Bob's lasers. For instance, increasing the intensity of the coherent state  $\langle \mu \rangle = 0.4 \rightarrow 0.6$  doubles the multi-photon emission probability. This enables Eve to circumvent the security provided by the no-cloning theorem and the decoy state method [6, 33–35].

Spectral attacks encompass two distinct scenarios: manipulating the frequency of the injected reference itself, and injecting additional optical signals at wavelengths far removed from the intended reference wavelength. While the former approach inevitably worsens the interference at the central node, thus enlarging the QBER, the latter exploits vulnerabilities arising from wavelength-dependent responses of the detectors and variations in attenuation across optical components within the system.

To mitigate these potential attacks, we recommend the use of monitoring detectors (“watchdogs”) strategically placed within the encoder setup, as illustrated in Fig. 1(b). A first watchdog placed before optical injection ensures the integrity of the incoming reference signal, while a second watchdog positioned immediately after the encoder monitors the output pulse train before attenu-

ation to the single-photon level, enabling classical-level signal processing. These watchdogs should continuously monitor power, timing, and spectral characteristics, triggering alerts upon detecting anomalies indicative of hardware malfunctions or potential eavesdropping attempts.

However, the design of these watchdogs requires careful consideration, as Eve could exploit their intrinsic limitations to evade detection [34]. For instance, slow photodetectors that integrate optical power over relatively long time intervals, compared to the encoding rate, might be sufficient to treat slow intensity fluctuations, but they will fail to detect rapid intensity modulations. Eve could maintain a constant average optical power, lowering and increasing the power within time windows shorter than the integration period, thus avoiding detection. Similarly, PDs with responsivity optimised for specific wavelengths (typically aligned with the intended communication wavelength) can be vulnerable to wavelength-dependent Trojan-horse attacks (THAs). Eve could impersonate Charlie by injecting alien signals at wavelengths outside the PD's detection range. In such scenarios, the watchdog would register only minimal increases in optical power, despite the presence of a high-intensity Trojan signal. This extrinsic signal could then propagate undetected through Alice's and Bob's setups, surviving the wavelength-dependent attenuation of critical optical components such as VOAs, intensity modulators, and phase modulators. Consequently, the Trojan wavelength signal could reach deep into the encoders, extracting sensitive information about the encoded quantum states (including intensity setting, basis choice, and

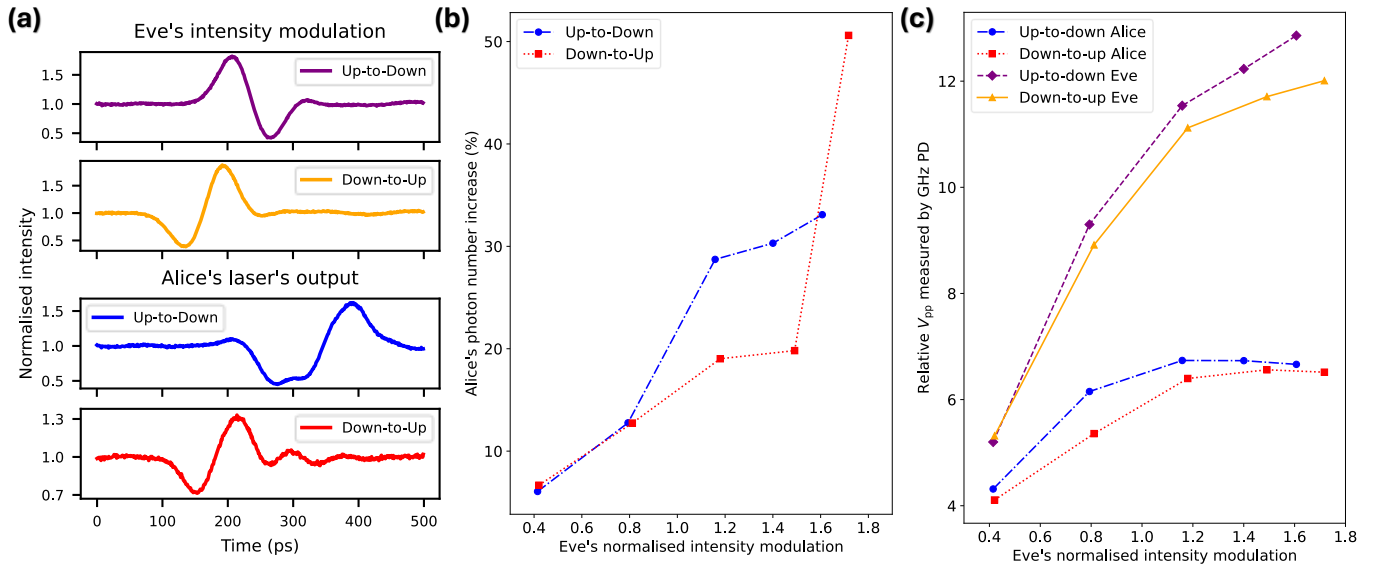


FIG. 3. **Detection performance of watchdog detectors under rapid intensity modulation attacks.** We study the attack under various amplitude modulations: “Eve’s normalised intensity modulation” in all sub-figures (and in Fig. 6) refers to the difference in power between the minima and maxima of the modulated laser signal (peak-to-peak), relative to the baseline power of the unmodulated signal. (a) Examples of the two primary intensity modulation patterns tested: “Up-to-Down” (power increased, then reduced) and “Down-to-Up” (power reduced, then increased), both maintaining constant average intensity. (b) SNSPD measurements showing a transient increase in mean photon number (up to 51%) during the modulation intervals. Slow-integrating power meters failed to detect these modulations. The abrupt increase at the final point of the “Down-to-Up” configuration is due to the merging between the main pulse and the trailing ringing. (c) fast-PD output reliably identifying all modulation types tested, enabling immediate attack detection and limiting adversarial interference to a denial-of-service scenario.

even bit choice) and leaking it back to Eve.

To accurately determine the required performance characteristics of these watchdogs and enhance their resilience, we experimentally recreated these attack scenarios under controlled conditions. Using detectors with different temporal and spectral responses, we evaluated the effectiveness of these attacks and established robust design criteria for the watchdogs, as presented in the following section.

## II. TEST OF THE SIDE CHANNELS AND COUNTERMEASURES

### A. Reference intensity modulation attack

In Fig. 2 we present the setup used to investigate the rapid intensity modulation attack, where Eve modulates only the intensity of the reference laser. Such signal is routed into Alice’s (equivalently, Bob’s) station, passing through a PC and a PBS to ensure a single polarisation, effectively converting polarisation-based attacks into intensity-based ones. A narrowband spectral filter is applied to reroute unwanted spectral components (see below) and isolate the expected reference wavelength, preventing injection of extrinsic light. The spectrally filtered signal is then used to injection-lock Alice’s laser, syn-

chronising its phase and frequency with the modulated reference. Importantly, all lasers operate in continuous wave (CW) mode, and the encoder and the rest of the components shown in Fig. 1(b) are omitted in the setup shown in Fig. 2. This is because the experiment focuses specifically on assessing how intensity modulation of the reference signal affects the OIL process, potentially compromising transmitter security.

Superconducting nanowire single-photon detectors (SNSPDs) equipped with a time tagger, together with an OSA, are used to characterise the properties of the modulated reference signal prior to locking of Alice’s laser, and second, to study the effects that the attack has on the effective photon numbers and the spectra of the locked laser.

The first option we investigate for a potential watchdog consists of two GHz-bandwidth PDs monitoring the high-speed behaviour of the system: the Injection PD tracks the temporal profile of the signal arriving at the encoder’s laser via the circulator, while the Locking PD observes the output of the laser after the locking process. The GHz bandwidth is chosen to match the state-of-the-art TF-QKD systems, which operate at GHz clock rates, defining the expected maximum encoding speed.

We compare these fast-PD’s results with those of a conventional slow-integrating power meter, monitoring both the power levels of the unfiltered optical signal and,

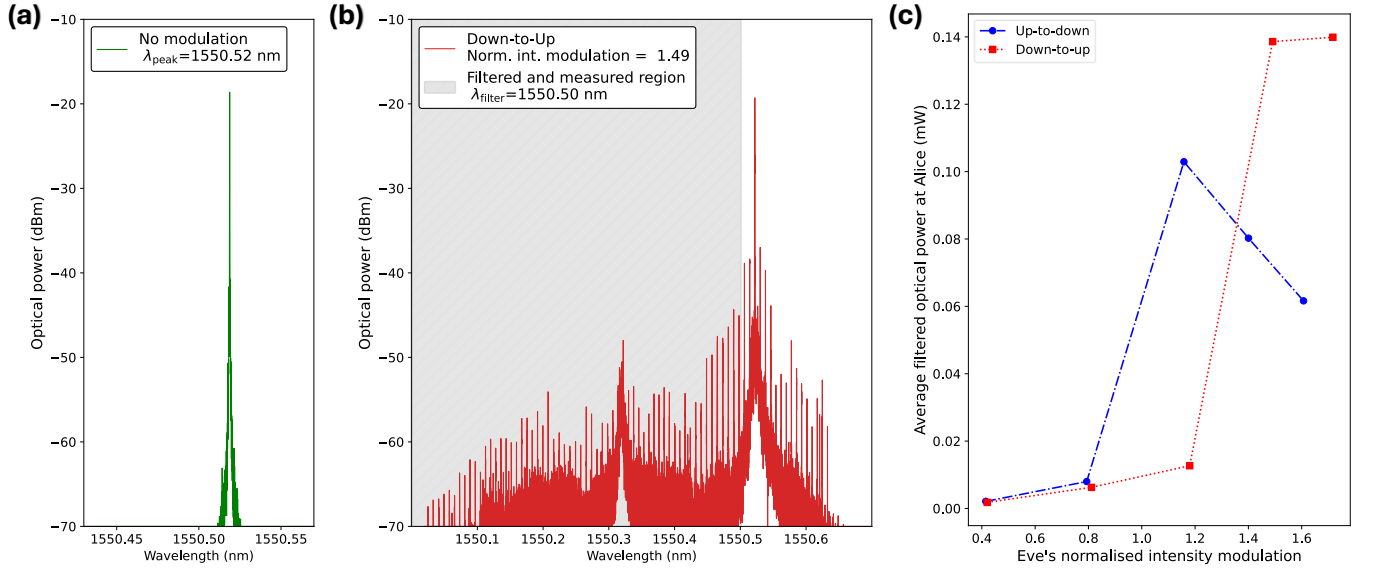


FIG. 4. **Spectral detection of intensity modulation attacks.** (a) Reference optical spectrum of Alice’s LD without modulation. (b) Spectrum under active rapid intensity modulation, showing prominent sidebands around the main wavelength. (c) Power detected in the filtered sidebands region using a slow (25  $\mu\text{s}$  integration) power meter. The observed increase in power clearly indicates modulation-induced spectral broadening, providing a simple yet effective secondary detection method. The decay observed towards the end results from variations in the sidebands moving outside the tunable filter’s passband; these features are also visible on the right side of the spectrum.

in conjunction with the filters, to detect power coming from extrinsic and unexpected wavelengths, both before and (more importantly) after the locking stage. Owing to amplitude–phase coupling in the laser’s gain medium, oscillations in the injected power convert partly into instantaneous frequency shifts, resulting into both intensity modulations and spectral sidebands. This spectral distortion in Alice’s local laser output provides another signature of malicious intervention, which can be detected as a countermeasure. To this end, the combined use of the slow-integrating power meter alongside spectral filters to detect unexpected wavelength components results in a secondary detection venue against intensity modulation attacks.

Since Eve’s optimal modulation strategy should aim to avoid detection by maintaining a constant average intensity, thus evading detection by slow integrating watchdogs, we consider two main modulation patterns (Fig. 3(a)): “Up-to-Down” (an increase followed by a reduction), and “Down-to-Up” (a reduction followed by an increase in optical power relative to a baseline). Detection results are displayed in Figs. 3(b) and 3(c), while an extensive overview of the pulse designing phase, together with additional modulation scenarios, can be found in Methods, and the Supplementary Material respectively.

The SNSPDs data in Fig. 3(b) indicates that Eve’s modulation can produce transient increases in the mean photon number by up to 51% during the modulated time intervals. This demonstrates that her injected intensity modulation attack is a credible threat, as it enables a controlled increase in the photon number emitted by Alice

or Bob. Its impact on the secret key rate (SKR) is quantified later. However, conventional power meters register no modulation when integrating in their fastest configuration of 25  $\mu\text{s}$ . The results of these measurements are in the Supplementary Material. Although we observe power meters to be oblivious to these modulations, we note that even if they could detect sustained increases or decreases in average power, Eve could strategically time the modulated pulses to dilute the fluctuations, making them indistinguishable from detector noise. Therefore, our analysis shows that slow-integrating power meters alone are insufficient against this type of attack. Nevertheless, as reported in Fig. 3(c), the fast-PDs reliably detect anomalies for every modulation tested, promptly identifying the attack, enabling countermeasures, and limiting Eve’s impact to a denial-of-service scenario since once the attack is detected the protocol should be interrupted.

For the results of the power meter aided by the spectral filters refer to Fig. 4. Comparing an unmodulated spectral baseline (Fig. 4(a)) with an active modulation scenario (Fig. 4(b)), clear sidebands emerge. A narrowband spectral filter directs these otherwise absent spectral sidebands into a power meter, providing a straightforward detection method even with slow integration times. The results of Fig. 4(c) were taken with the 25  $\mu\text{s}$  integration of the power meter, but are observable with integration times up to 100  $\mu\text{s}$ . This approach enables reliable identification of intensity modulation attacks by monitoring unexpected spectral shifts, enabling Alice and Bob to abort the QKD session for protection, since any increase in power in these wavelengths would be created by an at-

tack on the encoding laser.

#### Overestimation of the secret key rate

Crucially, underestimating the actual optical power emitted by Alice and Bob, even still under the single-photon regime, can lead to an overestimation of the achievable SKR. To illustrate this, we consider the “Sending-or-Not-Sending” TF-QKD protocol, and compute the asymptotic SKR in the presence of the attack (see Ref. [6] for the protocol description and security proof). The results of this analysis are presented in Fig. 5, with details about the simulations provided in the Supplementary Material.

To run the protocol, Alice and Bob must first optimise the key parameters (which, in the asymptotic regime, are the sending probability  $\tilde{\epsilon}$  and the signal intensity  $\tilde{\mu}$  of their coherent states), based on their system characteristics and channel conditions. This optimisation yields a theoretical estimate for the expected SKR (blue dotted curve in Fig. 5). Under Eve’s intensity modulation attack, however, the signal states they actually prepare have an intensity  $\tilde{\mu}' = \kappa\tilde{\mu}$ , where  $\kappa$  is an enhancement factor. Here we set  $\kappa = 1.51$ , corresponding to the maximum experimentally measured intensity increase (Fig. 3(b)). If Alice and Bob are aware of this increased intensity, they can correctly apply the security analysis, obtaining a lower bound on the SKR that accurately reflects the attack (green solid curve). Nevertheless, if they were oblivious to the attack and employed the expected intensity value  $\tilde{\mu}$  in the SKR calculation together with the actual statistics observed, they would retrieve an erroneous SKR which is higher than the actual one provided by the proof (red dashed line).

Fig. 5 demonstrates that, even in the asymptotic limit, there is a noticeable discrepancy in the SKR estimation under attack conditions. While a full security analysis accounting for finite-size effects is beyond the scope of this work, we note that such discrepancies become more pronounced in finite-key scenarios, as intensity modulation also impacts decoy states. In extreme cases with small data block sizes, this discrepancy could even surpass the theoretical upper bound on the SKR, yielding a completely insecure key rate [9, 35] estimate. Accurately bounding the emitted states’ intensity is critical to ensure practical security.

#### B. Trojan wavelength attack

We now move on to characterise the Trojan wavelength attack in the context of OIL TF-QKD, where we experimentally investigate the spectral response of the laser cavity itself. Critically, any Trojan wavelength injected into the encoder will undergo the same encoding steps, potentially leaking full information about the intensity and phase settings if not effectively filtered. It should

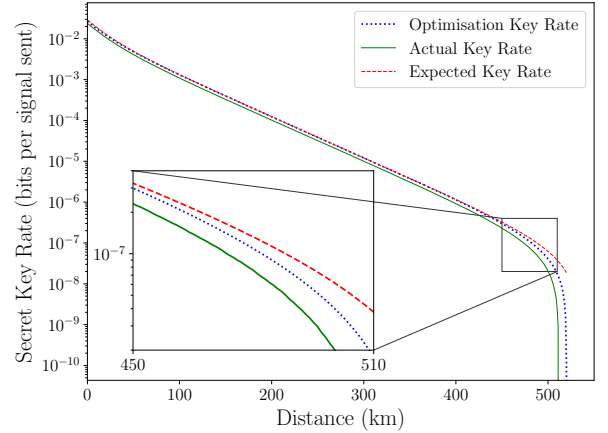


**FIG. 5. Impact of intensity modulation attacks on the estimated SKR in the Sending-or-Not-Sending TF-QKD protocol.** The blue dotted line shows the optimisation key rate that Alice and Bob simulate in realistic conditions to determine the optimal protocol parameters, while the green line shows the maximum SKR that the security proof can guarantee given the enhanced intensities (by 51%) of their pulses when under attack. The red line shows the SKR they would erroneously estimate given the detection statistics under attack, if the latter went unnoticed. Crucially, by obliviously sending higher intensities, Alice and Bob are overestimating the amount of secret key they can produce. Simulations are computed in the asymptotic regime, assuming infinite decoys. Details and parameters are provided in the Supplementary Material.

be noted that this component arrangement is unique to TF-QKD, as the reference signal reaches the LD via the circulator connected to the service channel, rather than from the quantum channel.

Previous studies have documented the spectral behaviour of common encoder components such as attenuators and modulators [36]. However, the response of a laser cavity under illumination by wavelengths far outside its typical operating band has not yet been characterised, particularly in the context of OIL architectures. As this is the fundamental missing piece to properly compute the total attenuation along the full optical path experienced by light at every wavelength, our setup (depicted in Fig. 6(a)) isolates the laser cavity using only a fibre-optic circulator and a distributed feedback (DFB) laser, deliberately omitting other encoder components in order to specifically analyse cavity interactions at out-of-band wavelengths. In doing so, we aim to reveal any previously unidentified spectral dependencies or unexpected vulnerabilities inherent in OIL-based TF-QKD architectures.

To explore a broad spectral region, we use a super-continuum wideband fibre laser covering a wavelength range of 500-2200 nm. While all encoder components are optimised for the telecom C-band centred around 1550 nm, we intentionally illuminate the DFB laser with

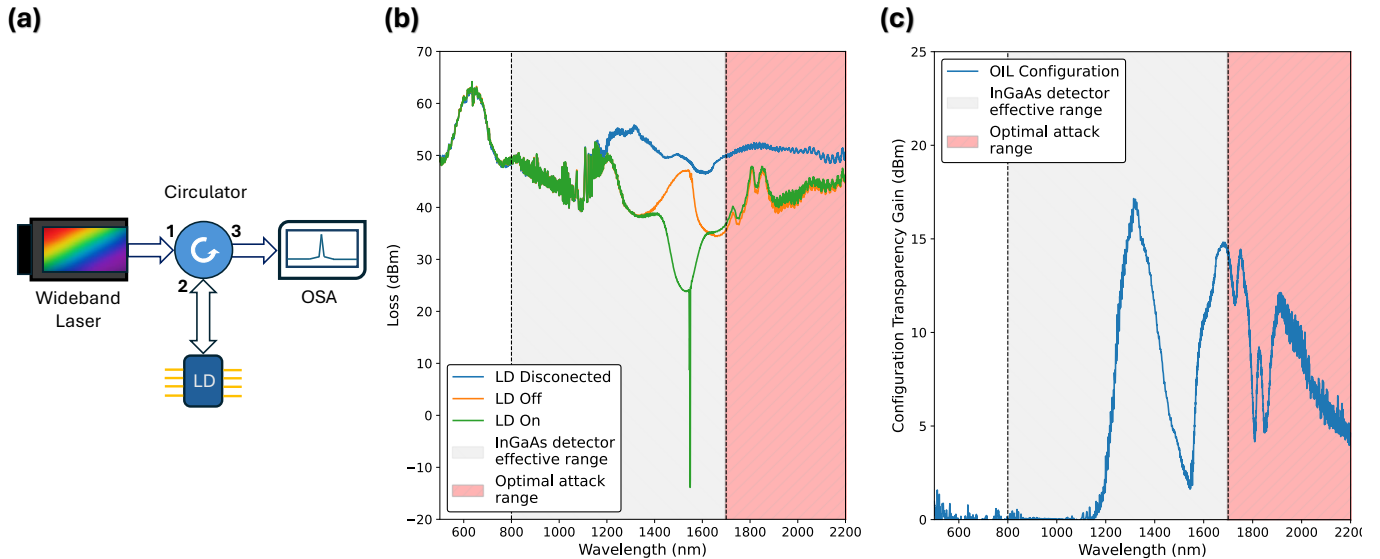


FIG. 6. **Spectral characterisation of laser cavity reflections relevant to Trojan wavelength attacks.** (a) Experimental setup for studying the Trojan wavelength attack. A wideband laser and an OSA are employed to characterise the spectral response of the LD over a broad wavelength range from 500 nm to 2200 nm. (b) Measured spectral losses for different experimental configurations of the encoder setup. Losses were determined by subtracting the spectra obtained with the wideband laser alone from those measured when the circulator and LD were connected. Three configurations are compared: circulator alone (no LD connected), circulator with LD connected but powered off, and circulator with LD connected and powered on. (c) Effective transparency gained in the whole Circulator-DFB LD configuration, computed as the difference between the losses with the LD disconnected and the LD connected but off. Results show significant deviation of the expected transparency due to reflections when the cavity is connected, and allow to determine the optimal wavelengths for the attack.

wavelengths far from its nominal injection locking region. Importantly, the laser under test does not have an isolator and is biased just above its lasing threshold, without attempting OIL at these out-of-band wavelengths. Reflected signals, largely bypassing the cavity due to off-resonance conditions, are collected via the circulator and measured using an OSA. Although different laser designs can have different reflectivity mirrors on its facets (or no mirror for the case with only broadband Fresnel reflection), they are all likely to reflect a portion of the incoming light. This arrangement allows us to directly measure and characterise how the laser cavity structure affects signals at wavelengths significantly outside its normal operational range, identifying spectral regions where unexpectedly high levels of reflected power could aid Eve's Trojan attack.

Figure 6(b) shows the spectral losses observed by comparing spectra from the wideband source alone to those from three different experimental configurations: circulator only (no LD connected), circulator with LD connected but powered off, and circulator with LD actively lasing. Conversely, Fig. 6(c) highlights the effective transmissivity gained through the presence of the LD cavity in the OIL configuration, calculated by comparing configurations with the LD connected and disconnected (LD off only). This approach reveals the ideal wavelengths to use for this attack. That is, those with positive transmissivity gains that are undetectable by typi-

cal watchdogs (like InGaAs PDs, which are optimised for  $\sim 1550$  nm and sharply lose responsivity beyond 1700 nm [37]), thus allowing the injected signals to bypass the cavity unnoticed.

The results in Fig. 6(c) clearly indicate significant cavity-induced reflections within 1200 nm to 2200 nm. Eve could exploit this broad spectral range to inject a high-power optical signal, with a wavelength significantly above what an InGaAs detector would detect. Under these conditions, the detected optical power would substantially underestimate the actual injected power, allowing Eve's Trojan signal to propagate through the encoder at classical power levels, despite the typical attenuation mechanisms implemented within quantum encoding setups.

These results illustrate how the Trojan wavelength attack must be carefully taken into account for the security of any OIL based TF-QKD system, as it allows to completely learn the encoding settings when overlooked. Fortunately, to prevent this attack one only requires an adequate amount of spectral filtering with high enough attenuation at these external wavelengths, thus ensuring that for optical frequencies outside of the locking range, the intensity of the light after the encoder is sufficiently weak to guarantee security.

In order to compute the required amount of attenuation one must understand what is the maximum amount of power that Eve could inject into Alice and Bob's de-

vices, as well as what is the maximum acceptable output power of the encoders, according to security proofs. For the former is typically considered, as a worse-case scenario, the so-called laser-induced damage threshold (LIDT). For light at telecom wavelengths, Ref. [32] reports a theoretical estimate of the LIDT value of 55kW, while in a recent certification guideline Ref. [24] considers as a more reasonable conservative assumption that the maximum possible insertion power for a realistic Eve is 100W. Note that this power threshold only applies to fibre, and does not take into consideration possible damage to connectors and other components, meaning that in practice it is probably still over-conservative.

Crucially, the value of the LIDT strongly depends on the wavelength [38]. Therefore, by assuming a LIDT of 100 W at  $\lambda_0 = 1550$  nm, the LIDT at an arbitrary wavelength  $\lambda$  can be found by following the square-root dependence as

$$\text{LIDT}(\lambda) = \sqrt{\frac{\lambda}{\lambda_0}} \times 100 \text{ W.} \quad (1)$$

Note that Eq. 1 suggests that the maximum amount of allowed input power for Eve is larger for longer wavelengths. This phenomenon must be properly considered when designing the attenuation scheme.

As for a bound on the maximum tolerable output power, a comprehensive analysis specific to TF-QKD has yet to be established. Nevertheless, since the Trojan wavelength attack is conceptually equivalent to the standard THA on prepare-and-measure QKD systems, the acceptable output intensities derived from security proofs for such schemes might serve as a rough estimate for the maximum allowed output power of a TF-QKD transmitter.

In general, an overall input-to-output optical isolation of approximately 200 dB is considered necessary to approach the performance of an ideal, leakage-free scenario [32, 39–44]. Such levels of attenuation can be achieved using off-the-shelf spectral filters, including multiple units in a cascaded configuration to provide the required out-of-band suppression.

### III. CONCLUSIONS

In this work, we have performed a detailed analysis of all possible degrees of freedom of the reference laser that could pose a security threat in OIL-based TF-QKD systems. We identified two new viable attack vectors: rapid intensity modulation of the injected reference, and Trojan signals at wavelengths well outside the optimal detection range of the watchdogs, equipped with sufficient power to pass through the system despite existing attenuation.

To counter external intensity modulation of the generated pulse train, we recommend the use of a fast-PD as a watchdog, ideally as fast as the encoding itself, in

order to take advantage of the fact that the reference signal is still at classical power levels before attenuation to the single-photon regime. Additionally, we propose placing a wide bandpass filter (say e.g. 0.05 nm) centred on the reference wavelength, with all sidebands redirected to a dedicated detector: as we have shown, this allows for detection of spectral fluctuations in the output of the encoder laser that are generated by the manipulation of the OIL.

Moreover, our results reveal that out-of-band reflections from the OIL cavity create a clear pathway for high-power Trojan signals. Fortunately, this vulnerability can be effectively neutralised with straightforward measures. By limiting incoming light exclusively to the spectral range of the watchdog PD, simple and commercially available optical filters can readily suppress any unintended wavelengths. These devices introduce minimal additional optical loss, typically in the order of a few tenths of a decibel, and can be seamlessly integrated into existing setups without substantial redesign.

This, coupled with a periodic spectral verification and monitoring of Alice and Bob's lasers, comprehensively address the identified vulnerabilities, significantly reinforcing the practical security of OIL-based TF-QKD systems without compromising their performance.

More broadly, our analysis emphasises the importance of restricting Eve's control over the degrees of freedom of the injected optical signals, such as frequency, power, temporal shape, and polarisation, to ensure robust security of quantum communication protocols. A rigorous and comprehensive restriction not only addresses currently identified attack vectors but also provides resilience against future, yet-undiscovered, attack strategies. Maintaining tight control over all optical parameters entering the encoder thus forms a foundational element for securing practical quantum communication systems in real-world deployments.

### DATA AND MATERIALS AVAILABILITY

All data are available from the corresponding author upon reasonable request.

### CORRESPONDENCE AND REQUESTS FOR MATERIALS

Should be addressed to S.J. at:  
sergio.juarez@toshiba.eu.

### AUTHORS CONTRIBUTIONS

S.J., A.M., R.I.W., and D.R. identified the academic motivation for this research project. S.J. and A.M. built the experimental setups, collected the measurements, and analysed the results with support and supervision

from M.P., R.I.W., T.D., R.M.S., and D.R., and particularly, derived the simulation results under the supervision of M.C.. S.J., A.M., and R.I.W. wrote the manuscript, with all authors contributing to its improvement and the verification of the results.

## ACKNOWLEDGMENTS

The authors thank S. Morrissey, F. Grünenfelder, O. Crampton, A. Brzosko, Y.S. Lo, G. Shooter, and P.R. Smith, for insightful discussions. We acknowledge support from the European Union's Horizon Europe Framework Programme under the Marie Skłodowska Curie Grant No. 101072637, Project Quantum-Safe Internet (QSI). Views and opinions expressed are however those of the author(s) only and do not necessarily reflect those of the European Union. Neither the European Union nor the granting authority can be held responsible for them. We also acknowledge support from the Galician Regional Government (consolidation of research units: atlanTTic), the Spanish Ministry of Economy and Competitiveness (MINECO), the Fondo Europeo de Desarrollo Regional (FEDER) through the grant No. PID2024-162270OB-I00, MICIN with funding from the European Union NextGenerationEU (PRTR-C17.I1) and the Galician Regional Government with own funding through the “Planes Complementarios de I+D+I con las Comunidades Autónomas” in Quantum Communication, the “Hub Nacional de Excelencia en Comunicaciones Cuánticas” funded by the Spanish Ministry for Digital Transformation and the Public Service and the European Union NextGenerationEU, the European Union's Horizon Europe Framework Programme under the project “Quantum Security Networks Partnership” (QSNP, grant agreement No 101114043) and the European Union via the European Health and Digital Executive Agency (HADEA) under the Project QuTechSpace (grant 101135225).

## COMPETING INTERESTS

The authors declare no competing interests.

## IV. METHODS

In this section we present the details of our investigation on the modulation parameters for Eve, and discuss how for every configuration a sufficiently high repetition rate deceives slowly-integrating power meters, which therefore constitute unsecure watchdogs.

Fig. 7 reports an example of input pattern for Eve's intensity modulator for the case of a “Up” modulation (that is, fast, periodic increases in the optical power of the reference signal), as well as for the “Up-to-down” modulation introduced in Fig. 3. The vertically mirrored patterns yield the “Down” and the “Down-to-up” configurations, respectively. For each

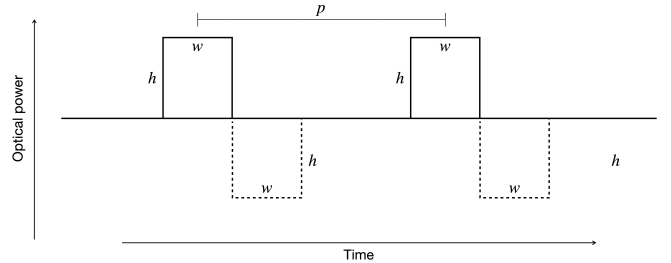


FIG. 7. **Modulation example of Eve's attack.** The schematics describe the nominal input provided to the Int. Mod. in Fig. 2. Solid lines refer to an “Up” configuration where Eve periodically increases the input power, whereas by appending to this modulation a symmetric reduction in power to keep the average power constant (dashed lines), Eve can prepare the “Up-to-down” configuration. The actual modulated signal in the latter case is displayed in the first plot of Fig. 3(a). The “Down” and “Down-to-up” configurations are obtained by considering vertical mirrored versions of these schemes. For each configuration we test different values of the pulse height  $h$ , the pulse width  $w$  and the modulation period  $p$ .

of the four configurations, we tested input and output statistics by changing the attack repetition rate (corresponding to  $1/p$  from Fig. 7) and the modulation width  $w$  and height  $h$ . Crucially, as noted in Fig. 3, for both the “Up-to-down” and “Down-to-up” modulations of the reference signal, the locked light at Alice's output always results in a “Down-to-up” configuration. This phenomenon also occurs for the “Up” and “Down” schemes, but notably in these latter cases the induced peak above the baseline is much smaller than the inflection below the baseline, resulting in a worse quality of the injection and overall reduction of the mean photon density. As this will affect performance rather than security, here we focus on the analysis for the “Up-to-down” and “Down-to-up” configurations, which allow instead to induce a significant transient increase in the optical power.

For the repetition rate of the attack we tested values ranging from 100MHz to 5GHz, comparable with the operational rate of state-of-the-art QKD schemes. For all these options it holds  $p \gg w$ , meaning that the produced pulse shape is not altered, and no appreciable changes have been observed in the detection statistics. Therefore, in this analysis we consider a modulation rate of 1GHz. As for the modulation width, we analysed the produced pulse shapes while sweeping over the range 50ps–250ps. We observed that a short modulation is preferable as it allows for a steeper transient between low and high levels of the photon density, which ultimately results in wider and taller peaks above the baseline. Therefore, results in this section refer to the setting choice  $w = 50$ ps, corresponding to the minimal resolution of our controls.

Finally, we tested various magnitudes of the modulation height  $h$ . Increasing this parameter directly impacts the modulation amplitude of the photon density. As this quantity is the most objective and meaningful metric for a device-agnostic analysis, figures in this paper show various experimental results as a function of Eve's normalised intensity modulation, corresponding to the peak-to-peak amplitude of the SNSPDs results displayed, for example, in Fig. 3(a).

The full experimental results for power meters are displayed

in Sec. S1 B of the Supplementary Material, where Figs. S1-S2 report the normalised average power and normalised power fluctuations detected by the devices, respectively, and compare them with the noiseless case (no attack).

Statistics are computed over  $\mathcal{O}(10^5)$  samples for each configuration. We observe that regardless of the attack intensity and integration time, power meters fail to detect anomalies in the observed quantities, thus mistakenly assuming a safe scenario when Alice's laser is under a modulation attack. This motivates us to introduce novel surveillance procedures, namely the countermeasures introduced in Sec. II A, so to guarantee the implementation security of OIL-based TF-QKD against this novel class of potential threats.

---

[1] C. H. Bennett and G. Brassard, *Theoretical Computer Science* **560**, 7 (2014).

[2] A. K. Ekert, *Physical Review Letters* **67**, 661 (1991).

[3] S. Pirandola, U. L. Andersen, L. Banchi, M. Berta, D. Bunandar, R. Colbeck, D. Englund, T. Gehring, C. Lupo, C. Ottaviani, J. L. Pereira, M. Razavi, J. Shamsul Shaari, M. Tomamichel, V. C. Usenko, G. Vallone, P. Villoresi, and P. Wallden, *Advances in Optics and Photonics* **12**, 1012 (2020).

[4] H.-K. Lo, M. Curty, and K. Tamaki, *Nature Photonics* **8**, 595 (2014).

[5] M. Lucamarini, Z. L. Yuan, J. F. Dynes, and A. J. Shields, *Nature* **557**, 400 (2018).

[6] X.-B. Wang, Z.-W. Yu, and X.-L. Hu, *Physical Review A* **98**, 10.1103/PhysRevA.98.062323 (2018).

[7] H. Xu, Z.-W. Yu, C. Jiang, X.-L. Hu, and X.-B. Wang, *Physical Review A* **101**, 10.1103/PhysRevA.101.042330 (2020).

[8] M. Curty, K. Azuma, and H.-K. Lo, *npj Quantum Information* **5**, 64 (2019).

[9] M. Curty, T. Moroder, X. Ma, H.-K. Lo, and N. Lütkenhaus, *Phys. Rev. A* **79**, 032335 (2009).

[10] S. Pirandola, R. Laurenza, C. Ottaviani, and L. Banchi, *Nature Communications* **8**, 15043 (2017).

[11] M. Minder, M. Pittaluga, G. L. Roberts, M. Lucamarini, J. F. Dynes, Z. L. Yuan, and A. J. Shields, *Nature Photonics* **13**, 334 (2019).

[12] M. Pittaluga, M. Minder, M. Lucamarini, M. Sanzaro, R. I. Woodward, M.-J. Li, Z. Yuan, and A. J. Shields, *Nature Photonics* **15**, 530 (2021).

[13] J.-P. Chen, C. Zhang, Y. Liu, C. Jiang, D.-F. Zhao, W.-J. Zhang, F.-X. Chen, H. Li, L.-X. You, Z. Wang, Y. Chen, X.-B. Wang, Q. Zhang, and J.-W. Pan, *Physical Review Letters* **128**, 180502 (2022).

[14] S. Wang, Z.-Q. Yin, D.-Y. He, W. Chen, R.-Q. Wang, P. Ye, Y. Zhou, G.-J. Fan-Yuan, F.-X. Wang, Y.-G. Zhu, P. V. Morozov, A. V. Divochiy, Z. Zhou, G.-C. Guo, and Z.-F. Han, *Nature Photonics* **16**, 154 (2022).

[15] Y. Liu, W.-J. Zhang, C. Jiang, J.-P. Chen, C. Zhang, W.-X. Pan, Di Ma, H. Dong, J.-M. Xiong, C.-J. Zhang, H. Li, R.-C. Wang, J. Wu, T.-Y. Chen, L. You, X.-B. Wang, Q. Zhang, and J.-W. Pan, *Physical Review Letters* **130**, 210801 (2023).

[16] M. Pittaluga, Y. S. Lo, A. Brzosko, R. I. Woodward, D. Scalcon, M. S. Winnel, T. Roger, J. F. Dynes, K. A. Owen, S. Juárez, *et al.*, *Nature* **640**, 911 (2025).

[17] J.-P. Chen, C. Zhang, Y. Liu, C. Jiang, W.-J. Zhang, Z.-Y. Han, S.-Z. Ma, X.-L. Hu, Y.-H. Li, H. Liu, F. Zhou, H.-F. Jiang, T.-Y. Chen, H. Li, L.-X. You, Z. Wang, X.-B. Wang, Q. Zhang, and J.-W. Pan, *Nature Photonics* **299**, 1476 (2021).

[18] H. Liu, C. Jiang, H.-T. Zhu, M. Zou, Z.-W. Yu, X.-L. Hu, H. Xu, S. Ma, Z. Han, J.-P. Chen, Y. Dai, S.-B. Tang, W. Zhang, H. Li, L. You, Z. Wang, Y. Hua, H. Hu, H. Zhang, F. Zhou, Q. Zhang, X.-B. Wang, T.-Y. Chen, and J.-W. Pan, *Physical Review Letters* **126**, 10.1103/PhysRevLett.126.250502 (2021).

[19] C. Clivati, A. Meda, S. Donadello, S. Virzì, M. Genovese, F. Levi, A. Mura, M. Pittaluga, Z. Yuan, A. J. Shields, M. Lucamarini, I. P. Degiovanni, and D. Calonico, *Nature Communications* **13**, 157 (2022).

[20] L. Zhou, J. Lin, Y. Jing, and Z. Yuan, *Nature Communications* **14**, 928 (2023).

[21] F. Xu, X. Ma, Q. Zhang, H.-K. Lo, and J.-W. Pan, *Reviews of Modern Physics* **92**, 131 (2020).

[22] V. Zapatero, Á. Navarrete, and M. Curty, *Advanced Quantum Technologies* **8**, 2300380 (2025).

[23] N. Jain, B. Stiller, I. Khan, D. Elser, C. Marquardt, and G. Leuchs, *Contemporary Physics* **57**, 366 (2016).

[24] V. Makarov, A. Abrikosov, P. Chaiwongkhon, A. K. Fedorov, A. Huang, E. Kiktenko, M. Petrov, A. Ponomosova, D. Ruzhitskaya, A. Tayduganov, D. Trefilov, and K. Zaitsev, *Phys. Rev. Appl.* **22**, 044076 (2024).

[25] Federal Office for Information Security (BSI), *Implementation Attacks against QKD Systems*, Tech. Rep. (Federal Office for Information Security (BSI), 2023) technical report.

[26] H.-K. Lo, M. Curty, and B. Qi, *Physical Review Letters* **108**, 130503 (2012).

[27] J. Ye, J.-L. Peng, R. J. Jones, K. W. Holman, J. L. Hall, D. J. Jones, S. A. Diddams, J. Kitching, S. Bize, J. C. Bergquist, L. W. Hollberg, L. Robertsson, and L.-S. Ma, *Journal of the Optical Society of America B* **20**, 1459 (2003).

[28] L. C. Comandar, M. Lucamarini, B. Fröhlich, J. F. Dynes, Z. Yuan, and A. J. Shields, *Optics express* **24**, 17849 (2016).

[29] T. K. Paraïso, R. I. Woodward, D. G. Marangon, V. Lovic, Z. Yuan, and A. J. Shields, *Advanced Quantum Technologies* **4**, 2100062 (2021).

[30] H. Du, T. K. Paraïso, M. Pittaluga, Y. S. Lo, J. A. Dolph, and A. J. Shields, *Optica* **11**, 1385 (2024).

[31] Q. Peng, J.-P. Chen, T. Xing, D. Wang, Y. Wang, Y. Liu, and A. Huang, *npj Quantum Information* **11**, 7 (2025).

[32] M. Lucamarini, I. Choi, M. B. Ward, J. F. Dynes, Z. L. Yuan, and A. J. Shields, *Phys. Rev. X* **5**, 031030 (2015).

[33] H.-K. Lo, X. Ma, and K. Chen, *Physical Review Letters* **94**, 230504 (2005).

[34] S. Sajeed, I. Radchenko, S. Kaiser, J.-P. Bourgoin, A. Pappa, L. Monat, M. Legré, and V. Makarov, *Phys. Rev. A* **91**, 032326 (2015).

[35] A. Huang, A. Navarrete, S.-H. Sun, P. Chaiwongkhon, M. Curty, and V. Makarov, *Phys. Rev. Appl.* **12**, 064043 (2019).

---

- [36] H. Tan, M. Petrov, W. Zhang, L. Han, S.-K. Liao, V. Makarov, F. Xu, and J.-W. Pan, arXiv preprint arXiv:2508.15136 (2025).
- [37] Thorlabs inc. s154c photodiode power sensor specifications (accessed 3 Jun 2025).
- [38] C. W. Carr, H. B. Radousky, and S. G. Demos, *Phys. Rev. Lett.* **91**, 127402 (2003).
- [39] G. Currás-Lorenzo, M. Pereira, G. Kato, M. Curty, and K. Tamaki, Security of high-speed quantum key distribution with imperfect sources (2025), arXiv:2305.05930 [quant-ph].
- [40] K. Tamaki, M. Curty, and M. Lucamarini, *New Journal of Physics* **18**, 065008 (2016).
- [41] W. Wang, K. Tamaki, and M. Curty, *New Journal of Physics* **20**, 083027 (2018).
- [42] A. Navarrete and M. Curty, *Quantum Science and Technology* **7**, 035021 (2022).
- [43] G. Currás-Lorenzo, A. Navarrete, J. Núñez-Bon, M. Pereira, and M. Curty, *Quantum Science and Technology* **10**, 035031 (2025).
- [44] X. Sixto, Á. Navarrete, M. Pereira, G. Currás-Lorenzo, K. Tamaki, and M. Curty, *Quantum Science and Technology* **10**, 035034 (2025).

## S1. SUPPLEMENTARY MATERIALS

### A. Simulation details

Here we present the details of the SKR simulations displayed in Fig. 5 of the main text. Our analysis is based on the protocol description and security proof for the “Sending-or-Not-Sending” (SNS) TF-QKD scheme introduced in Ref. [6] and the simulations provided in Ref. [8]. For simplicity, we consider the asymptotic case of infinitely many signals sent and infinitely many decoy intensities: the former implies that we can consider the key basis ( $Z$ -basis) to be chosen with probability  $P_Z \rightarrow 1$ , while the second implies that all the required yields can be computed exactly. In addition, we consider a standard channel model, where losses are modelled as a beam splitter whose transmittance matches the one of the optical fibre.

Let  $\eta$  denote the total channel transmittance for a given distance between Alice and Bob and let  $t = \sqrt{\eta}$  be the transmittance of the symmetric channels connecting each of the legitimate parties to Charlie. Here we consider a standard fibre loss coefficient  $\alpha = 0.2\text{dB/km}$  and detectors with dark count probability  $p_d = 10^{-8}$  and perfect detection efficiency (note that a finite detection efficiency could be incorporated in the definition of  $\eta$ ). Following the definition of key events in Ref. [6], the vacuum and single-photon yields are found to be respectively [6, 8]

$$s_0 = 2p_d(1 - p_d), \quad (2)$$

$$s_1 = 2(1 - p_d) \left[ p_d(1 - t) + \frac{t}{2} \right]. \quad (3)$$

Let  $\mu$  denote the intensity of the coherent state in the  $Z$  basis and  $\epsilon$  the probability of Alice and Bob sending such coherent state (instead of vacuum) when they select a key round. For the total yield of correct and erroneous bits in the  $Z$ -basis, we have

$$S_z^{\text{corr}} = 4\epsilon(1 - \epsilon)(1 - p_d)e^{-\mu t} \left( p_d + e^{\mu t/2} - 1 \right), \quad (4)$$

$$S_z^{\text{err}} = 2\epsilon^2(1 - p_d)e^{-2\mu t} \left( p_d + e^{\mu t} I_0(\mu t \cos(\Delta\varphi)) - 1 \right) + 2(1 - \epsilon)^2 p_d(1 - p_d), \quad (5)$$

where  $\Delta\varphi$  quantifies the polarisation misalignment and  $I_0(x)$  denotes the modified Bessel function of the first kind and order zero. It follows that for the total  $Z$ -basis yield and QBER we have:

$$S_z = S_z^{\text{corr}} + S_z^{\text{err}}, \quad E_z = \frac{S_z^{\text{err}}}{S_z}. \quad (6)$$

We remark that in the SNS-TF-QKD protocol the notion of a valid  $X$ -basis event, required to estimate the phase error rate using decoy states, is different from that of a  $Z$ -basis event. In detail, considering a decoy-state intensity  $\nu$ , we have that

$$S_x^{\text{corr}} = (1 - p_d) \left[ e^{-\nu t(1 - \cos(\Delta\varphi) \cos(\Delta\theta))} - (1 - p_d)e^{-2\nu t} \right], \quad (7)$$

$$S_x^{\text{err}} = (1 - p_d) \left[ e^{-\nu t(1 + \cos(\Delta\varphi) \cos(\Delta\theta))} - (1 - p_d)e^{-2\nu t} \right], \quad (8)$$

being  $\Delta\theta$  the phase misalignment. The total  $X$ -basis yield and QBER follow as

$$S_x = S_x^{\text{corr}} + S_x^{\text{err}}, \quad E_x = \frac{S_x^{\text{err}}}{S_x}. \quad (9)$$

From these quantities, an upper bound on the phase error rate can be found to be [6]:

$$e_{\text{ph}} \leq \bar{e}_{\text{ph}} = \frac{S_x E_x - \frac{1}{2} s_0 e^{-2\nu}}{2\nu e^{-2\nu} s_1}. \quad (10)$$

The above bound holds for any value of  $\nu$  and one can numerically check that it gets tighter as  $\nu \ll 1$ . Therefore, in our calculations we considered the fixed value of  $\nu = 10^{-6}$ .

Finally, the secret key rate  $R$  can be obtain as

$$R = 2\epsilon(1 - \epsilon)\mu e^{-\mu} s_1 [1 - h(\bar{e}_{\text{ph}})] - f_E S_z h(E_z), \quad (11)$$

where  $h(x)$  denotes the binary entropy of  $x$ .

As discussed in Sec. II A of the main text, before *actually* running the protocol Alice and Bob establish the optimal key parameters

$$(\tilde{\epsilon}, \tilde{\mu}) := \underset{\epsilon, \mu}{\text{argmax}} R \quad (12)$$

for a given set of system parameters  $\eta, p_d, \Delta\varphi$  and  $\Delta\theta$ . All curves in Fig. 5 of the main text refer to the optimal case  $\Delta\varphi = \Delta\theta = 0$ , but no significant difference has been observed when comparing to higher misalignment cases.

Due to the attack, although Alice and Bob *expect* to prepare  $Z$ -states with intensity  $\tilde{\mu}$  they *actually* prepare states with intensity  $\tilde{\mu}' = \kappa\mu$ , for some  $\kappa > 0$  ( $\kappa = 1.51$  in our case, from Fig. 3 of the main text). With a noiseless channel model, the  $Z$ -basis statistics that Alice and Bob *actually* observe are obtained through Eqs. 4, 5 and 6 with  $\mu = \tilde{\mu}'$ . This shows that

within this framework the attack has a direct impact on the  $Z$ -basis QBER, while its effect on the phase error rate is negligible as  $\nu \approx 0$ .

The *actual* secret key rate guaranteed by the security proof in this case is obtained by plugging in the *actual* intensity sent  $\tilde{\mu}'$  and the *actual* bit error rate  $E_z$  in Eq. 11, together with the sending probability  $\tilde{\epsilon}$  which is unchanged.

Nevertheless, if Alice and Bob are unaware of the attack, they believe they are sending coherent states with the average intensity  $\tilde{\mu}$  and observe the actual bit error rate  $E_z$ , as determined from Charlie's announcements. As a result, they compute their expected key rate by substituting  $\tilde{\mu}$  and  $E_z$  into Eq. 11, which leads to an erroneous overestimation.

## B. Power meters measurements

Here we report the power meters measurement data, as discussed in Sec. IV of the paper.

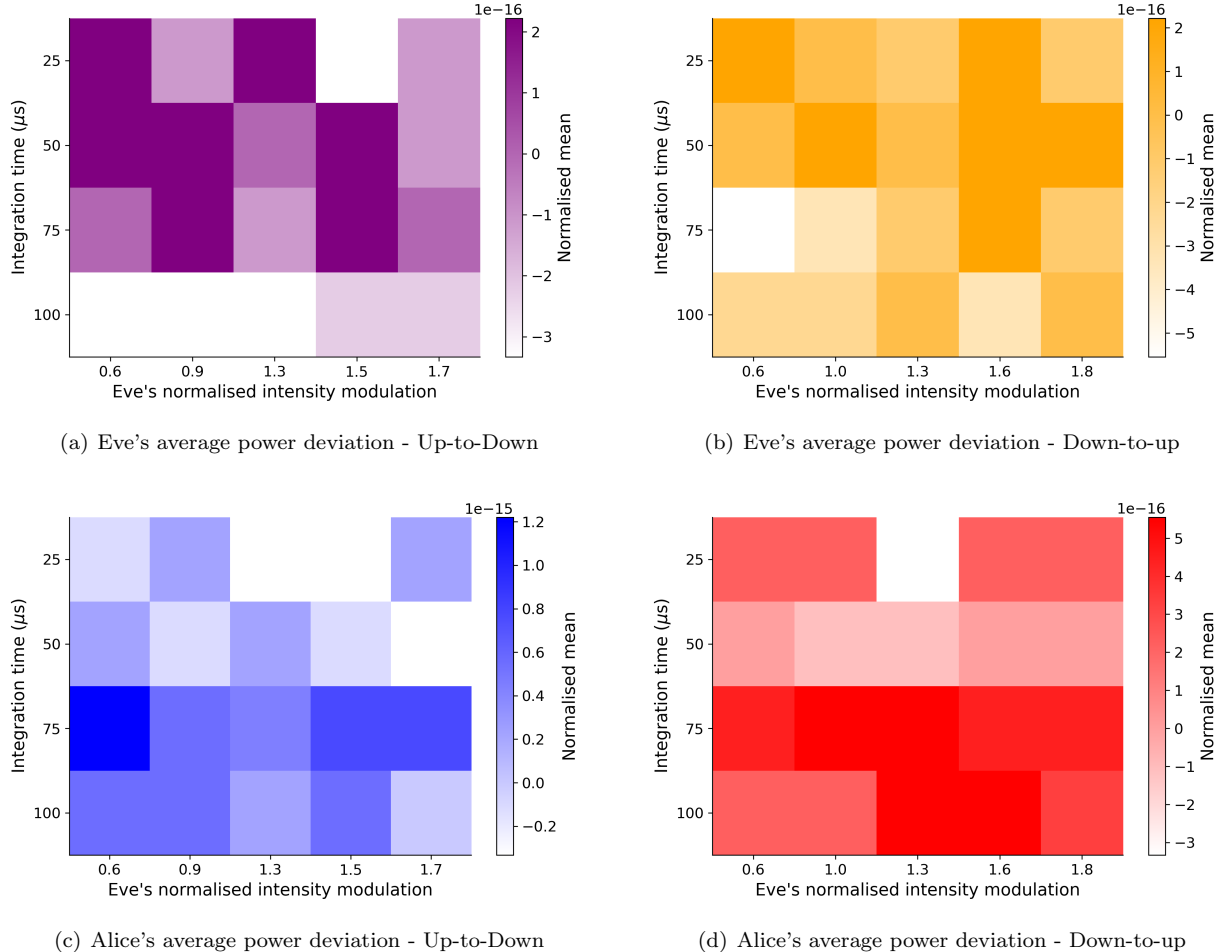


**FIG. S1. Power meters results - deviation of the average optical power under attack, with respect to the noiseless scenario.** These plots display the average recorded optical power of the signal for different integration periods of the power meters, upon changing the magnitude of the attack. The  $x$ -coordinate corresponds to the normalised peak-to-peak amplitude of the injected modulation (see e.g., Fig. 3(a)). For each configuration, the average power is normalised to its mean valued and compared with the average measurement of the power meter when the modulation is turned off, for each integration time. Results show that, over a few seconds of data acquisition, power meters are incapable of detecting power oscillations happening on a time scale up to two orders of magnitude smaller.

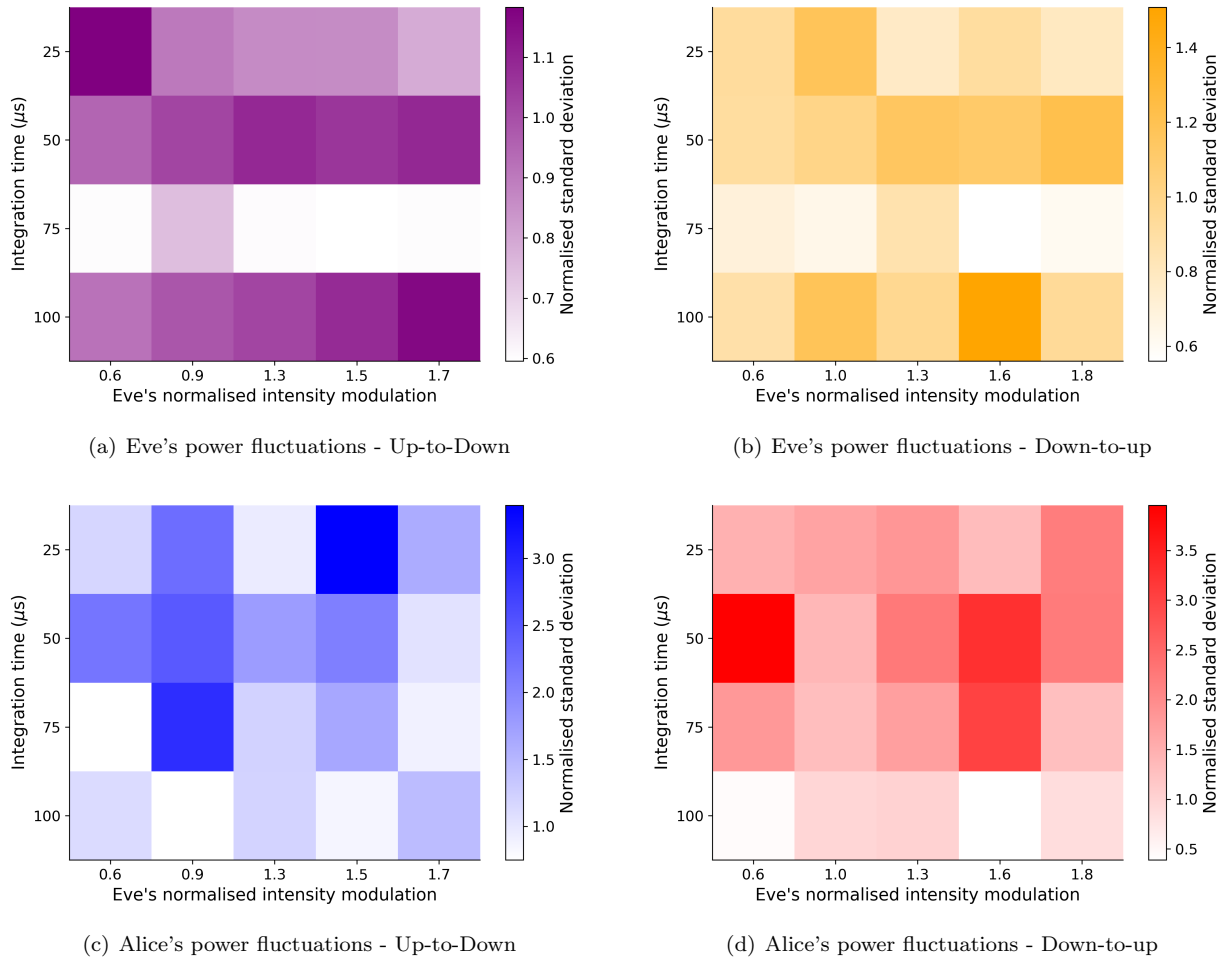


**FIG. S2. Power meters results - power fluctuations under attack, with respect to the noiseless scenario.** These plots display the standard deviation of the recorded optical power for different integration periods of the power meters, upon changing the magnitude of the attack. The  $x$ -coordinate corresponds to the normalised peak-to-peak amplitude of the injected modulation (see e.g., Fig. 3(a)). For each configuration, we compute the standard deviation of the optical power normalised to its mean value. Data are reported in units of the the standard deviation of the noiseless case, corresponding to the power meter measurements when the modulation is turned off. While for some particular parameter combinations the power fluctuations induced by the modulation on Alice's laser surpasses the expected one, in most cases power fluctuations are comparable with the noiseless scenario, meaning that the attack can go on unnoticed.